Assessing the quality of relaxation-time approximations with fully automated computations of phonon-limited mobilities

Romain Claes, Guillaume Brunin, Matteo Giantomassi, Gian-Marco Rignanese, and Geoffroy Hautier

Phys. Rev. B **106**, 094302 — Published 6 September 2022

DOI: 10.1103/PhysRevB.106.094302

Assessing the quality of relaxation-time approximations with fully-automated computations of phonon-limited mobilities

Romain Claes[1], Guillaume Brunin[1], Matteo Giantomassi[1], Gian-Marco Rignanese[1], and Geoffroy Hautier[1,2]*
[1] *UCLouvain, Institute of Condensed Matter and Nanosciences (IMCN), Chemin des Étoiles 8, B-1348 Louvain-la-Neuve, Belgium and*
[2] *Thayer School of Engineering, Dartmouth College, Hanover, New Hampshire 03755, USA*
(Dated: August 17, 2022)

The mobility of carriers, as limited by their scattering with phonons, can now routinely be obtained from first-principles electron-phonon coupling calculations. However, so far, most computations have relied on some form of simplification of the linearized Boltzmann transport equation based on either the self-energy, the momentum- or constant relaxation time approximations. Here, we develop a high-throughput infrastructure and an automatic workflow and we compute 67 phonon-limited mobilities in semiconductors. We compare the results resorting to the approximations with the exact iterative solution. We conclude that the approximate values may deviate significantly from the exact ones and are thus not reliable. Given the minimal computational overhead, our work encourages to rely on this exact iterative solution.

Carrier mobility is one of the most important characteristics of semiconductor materials and is a key property in many applications such as transistors, solar cells, thermoelectrics, transparent conductors, and light-emitting devices. Having reliable and efficient methods for computing these properties from first principles is therefore of crucial importance to improve the predictive power of *in silico* design methods. Despite significant progress in the field since the late 2000s, very few bulk semiconductors have been investigated so far due to the complexity of the problem associated with the inherent large computational cost. Only recently, efficient implementations such as EPW [1, 2], PERTURBO [3], and ABINIT [4–7], have allowed the community to report *ab initio* phonon-limited mobilities for a small set of semiconductors [8]. These methods are all based on density-functional theory (DFT) for ground-state properties and density-functional perturbation theory (DFPT) for vibrational properties [9, 10]. They all rely on Fourier-based interpolation schemes for the electron-phonon (e-ph) coupling matrix elements as the microscopic description of e-ph scattering processes requires a very dense sampling of the whole Brillouin zone (BZ) that is unrealistic for DFPT calculations. Recently, another methodology has been proposed with AMSET [11] where low-cost first-principles inputs are used to define models for acoustic deformation potential, piezoelectric and polar optical phonon scattering. This approach effectively enables faster evaluations of phonon-limited mobilities although not all the microscopic processes are explicitly accounted for with *ab initio* quality.

In all these state-of-the-art methods, transport properties are usually computed within the linearized Boltzmann transport equation (BTE), where carriers are described in terms of wave packets that propagate according to the semi-classical equations of motion between two consecutive scattering events. In principle, a fully *ab initio* description of transport phenomena should take into account several different scattering channels due to the interaction with, e.g., phonons, electrons, crystalline defects, ionized impurities, and even grain-boundaries in the case of polycrystalline samples. In practice, most of the studies reported so far have focused on the contribution due to e-ph scattering. In a few works, though, other effects such as the scattering by ionized impurities were also accounted for either in an indirect way via semi-empirical models [11, 12] or via additional *ab initio* calculations [13–15]. At the level of the e-ph scattering, the predictive power of *ab initio* methods has recently been quantified by estimating the impact of various effects such as spin-orbit coupling or many-body corrections to the e-ph vertex or effective masses in the case of silicon [12]. Even though a fully-microscopic theory of transport properties should take all these effects into account, it should be noted that such corrections are usually applied within a given approximation to the BTE, usually based on a relaxation time ansatz. However, in the few cases (GaAs [16], SnSe [17], and boron-V compounds [18]) for which the appropriateness of the popular approximations to the BTE has been quantified, some limitations of these approximations were already identified. Here, we assess their quality in a quantitative and systematic way using a computational workflow that allows us to investigate 67 phonon-limited mobilities among 54 semiconductors under different relaxation-time approximations in a completely automated way.

The derivation of the BTE can be found in many publications such as Refs. [8, 12, 19, 20]. In what follows, we summarize the most important equations and focus on electrons for the sake of brevity. Similar expressions can be easily obtained for holes. Atomic units are used everywhere unless stated otherwise. In semiconductors, the electron mobility ($\boldsymbol{\mu}_e$) is obtained by renormalizing the conductivity by the carrier concentration (n_e) and

* Corresponding author: geoffroy.hautier@dartmouth.edu

considering only the states in the conduction band (CB):

$$\mu_{e,\alpha\beta} = \frac{-1}{\Omega n_e} \sum_{n\in \mathrm{CB}} \int_{\mathrm{BZ}} \frac{d\mathbf{k}}{\Omega_{\mathrm{BZ}}} \frac{\partial f_{n\mathbf{k}}}{\partial \mathcal{E}_\beta} \mathrm{v}_{n\mathbf{k},\alpha}, \tag{1}$$

with α and β the Cartesian coordinates, Ω the volume of the unit cell, Ω_{BZ} the volume of the first Brillouin zone (BZ), n the electronic band index, $\mathbf{k}$ the wave vector, $f_{n\mathbf{k}}$ the occupation of the state in the steady configuration, $\boldsymbol{\mathcal{E}}$ the electric-field, and $\mathbf{v}_{n\mathbf{k}}$ the group velocity given by $\mathbf{v}_{n\mathbf{k}} = \nabla_{\mathbf{k}} \varepsilon_{n\mathbf{k}}$, where $\varepsilon_{n\mathbf{k}}$ is the band structure of the material. If we limit the discussion to drift mobilities where carriers are moving under the action of an electric field only (to the contrary of the Hall mobilities that also include the effect of a magnetic field), the $\partial f_{n\mathbf{k}}/\partial \mathcal{E}_\beta$ term entering Eq. (1) is the solution of the following linear integral equation

$$\begin{aligned}\frac{\partial f_{n\mathbf{k}}}{\partial \mathcal{E}_\beta} = \frac{\partial f^0_{n\mathbf{k}}}{\partial \varepsilon} \mathrm{v}_{n\mathbf{k},\beta} \tau^0_{n\mathbf{k}} + 2\pi \tau^0_{n\mathbf{k}} \sum_{m,\nu} \int_{\mathrm{BZ}} \frac{d\mathbf{q}}{\Omega_{\mathrm{BZ}}} |g_{mn\nu}(\mathbf{k},\mathbf{q})|^2 \\ \times \left[(n^0_{\mathbf{q}\nu} + f^0_{n\mathbf{k}}) \delta(\varepsilon_{n\mathbf{k}} - \varepsilon_{m\mathbf{k}+\mathbf{q}} - \omega_{\mathbf{q}\nu}) \right. \\ \left. + (n^0_{\mathbf{q}\nu} + 1 - f^0_{n\mathbf{k}}) \delta(\varepsilon_{n\mathbf{k}} - \varepsilon_{m\mathbf{k}+\mathbf{q}} + \omega_{\mathbf{q}\nu}) \right] \frac{\partial f_{m\mathbf{k}+\mathbf{q}}}{\partial \mathcal{E}_\beta},\end{aligned} \tag{2}$$

where $\tau^0_{n\mathbf{k}}$, that has the dimension of time, is given by

$$\begin{aligned}\frac{1}{\tau^0_{n\mathbf{k}}} = 2\pi \sum_{m,\nu} \int \frac{d\mathbf{q}}{\Omega_{\mathrm{BZ}}} |g_{mn\nu}(\mathbf{k},\mathbf{q})|^2 \\ \times \left[(n^0_{\mathbf{q}\nu} + f^0_{m\mathbf{k}+\mathbf{q}}) \delta(\varepsilon_{n\mathbf{k}} - \varepsilon_{m\mathbf{k}+\mathbf{q}} + \omega_{\mathbf{q}\nu}) \right. \\ \left. + (n^0_{\mathbf{q}\nu} + 1 - f^0_{m\mathbf{k}+\mathbf{q}}) \delta(\varepsilon_{n\mathbf{k}} - \varepsilon_{m\mathbf{k}+\mathbf{q}} - \omega_{\mathbf{q}\nu}) \right].\end{aligned} \tag{3}$$

In Eqs. (2)-(3), $f^0_{n\mathbf{k}}$ is the equilibrium Fermi-Dirac occupation function, $n^0_{\mathbf{q}\nu}$ is the Bose-Einstein distribution for the phonon of wave vector $\mathbf{q}$, mode index ν and frequency $\omega_{\mathbf{q}\nu}$, and $g_{mn\nu}(\mathbf{k},\mathbf{q})$ are the e-ph coupling matrix elements defined as $g_{mn\nu}(\mathbf{k},\mathbf{q}) = \langle \psi_{m\mathbf{k}+\mathbf{q}} | \Delta_{\mathbf{q}\nu} V^{\mathrm{KS}} | \psi_{n\mathbf{k}} \rangle$, where $\psi_{n\mathbf{k}}$ and $\psi_{m\mathbf{k}+\mathbf{q}}$ are the Kohn-Sham (KS) Bloch states and $\Delta_{\mathbf{q}\nu} V^{\mathrm{KS}}$ is the phonon-induced variation of the self-consistent KS potential [4, 5, 21].

Once discretized in the BZ, Eq. (2) becomes a system of linear equations that can be solved via iterative solvers (IBTE) that take advantage of the sparsity of the scattering operator to reduce both memory and computational cost. The main difficulty encountered when solving Eq. (2) is that very fine homogeneous $\mathbf{k}$-point meshes are required to account for the coupling among all the $\partial f_{n\mathbf{k}}/\partial \mathcal{E}_\beta$ terms and to properly converge transport properties. For this reason, in many studies the full solution of the BTE is usually replaced by the so-called self-energy relaxation time approximation (SERTA), where the second term on the right-hand side of Eq. (2) is completely neglected. This leads to an explicit expression for $\partial f_{n\mathbf{k}}/\partial \mathcal{E}_\beta$ in terms of other quantities readily available. In physical terms, this simplification corresponds to the relaxation time approximation (RTA) in which carriers are assumed to relax to the equilibrium Fermi-Dirac distribution $f^0_{n\mathbf{k}}$ with an exponential law and time constant $\tau^0_{n\mathbf{k}}$ when the external fields (electric and/or magnetic) are switched off. Inserting this approximated solution in Eq. (1) gives:

$$\mu^{\mathrm{SERTA}}_{e,\alpha\beta} = \frac{-1}{\Omega n_e} \sum_{n\in \mathrm{CB}} \int_{\mathrm{BZ}} \frac{d\mathbf{k}}{\Omega_{\mathrm{BZ}}} \frac{\partial f^0_{n\mathbf{k}}}{\partial \varepsilon_{n\mathbf{k}}} \mathrm{v}_{n\mathbf{k},\alpha} \mathrm{v}_{n\mathbf{k},\beta} \tau^0_{n\mathbf{k}}. \tag{4}$$

The SERTA acronym stems from the fact that $\tau^0_{n\mathbf{k}}$ is related to the inverse of the imaginary part of the e-ph Fan-Migdal self-energy [4, 21] that gives the lifetime of a *charged* quasi-particle excitation due to e-ph interactions. In other words, the SERTA uses a relaxation-time ansatz to approximate the true solution of Eq. (2) and assumes the transport relaxation time to be equal to the lifetime of a charged excitation. This is a reasonable but not necessarily correct assumption, especially because neglecting the second term on the right-hand side of Eq. (2) corresponds to ignoring all the processes in which carriers are scattered back into the state $n\mathbf{k}$ [8]. In more geometrical words, the SERTA always underestimates the mobility because it does not differentiate between forward and backward scattering even though forward scattering (small angle between $\mathbf{v}_{\mathbf{k}}$ and $\mathbf{v}_{\mathbf{k}+\mathbf{q}}$) does not deteriorate the mobility as much as backward scattering [22]. Unlike thermal transport where heat exchange occurs during all scatterings, electric current scattering is much more efficient when the direction of electron flow is altered [23, 24]. These back-scattering events can be partially accounted for using the momentum-relaxation time approximation (MRTA) whereby the integrand in Eq. (3) is now weighted by the efficiency factor [8, 11, 25, 26]

$$\alpha^{\mathrm{MRTA}}_{mn}(\mathbf{k},\mathbf{q}) = \left(1 - \frac{\mathbf{v}_{n\mathbf{k}} \cdot \mathbf{v}_{m\mathbf{k}+\mathbf{q}}}{|\mathbf{v}_{n\mathbf{k}}|^2} \right). \tag{5}$$

Indeed, this favors forward scattering geometrically and, therefore, the relative changes in the electron velocity due to the scattering processes are better taken into account. Finally, an even more crude approximation consists in assuming that the relaxation times are constant for all $n\mathbf{k}$, *i.e.* $\tau_{n\mathbf{k}} = \tau$ in Eq. (4). In this constant relaxation time approximation (CRTA), the mobility depends only on the band structure and on τ as a phenomenological parameter. Since the computation of phonons and e-ph matrix elements are not needed, this greatly reduces the computational cost. This is the main reason why the CRTA has been widely employed in the past. In particular, it has been implemented in BOLTZTRAP [27, 28] and extensively used, for instance to rank large sets of materials using a common lifetime [29–32] (or, equivalently, by looking at the transport effective mass [33, 34]). Another application lies in understanding experimental results by determining the lifetime in a specific material [28, 35, 36].

All these expressions have been implemented in the transport module of ABINIT. Our approach, detailed in

Ref. [4], takes advantage of (i) the tetrahedron integration scheme to reduce the number of e-ph transitions to be computed, (ii) a Fourier interpolation of the scattering potentials in **q** space including the proper treatment of dipole and quadrupole contributions, and (iii) exact KS wavefunctions that are computed only for the **k**-points lying inside a small energy window around the band edges. This procedure allows us to bypass the generation of maximally-localized Wannier functions, a major advantage in our context as all the steps of our workflow can be easily automated.

Even though the CRTA, SERTA, and MRTA have been widely used in the literature to characterize the transport of electrons or holes, the validity of such approximations has not yet been tested in a systematic way. Here, we analyze the phonon-limited transport in 54 different semiconductors, including 54 electron and 13 hole mobilities. This allows us to directly probe the quality of these different approximations to the IBTE. These 54 semiconductors have been selected by the following procedure. In order to reduce the total computation time, we consider only those semiconductors for which phonon properties are available in the Materials Project database [37, 38] and discard materials with imaginary phonon frequencies (vibrational instabilities) or those that are predicted to be thermodynamically unstable, *i.e.* with an energy above hull larger than 50 meV/atom. The results of Ref. [30] have then been used to remove all materials for which the average transport effective mass is larger than one. Finally, we enforce two additional constraints that are needed in order to be compatible with the previous DFPT calculations performed with PBEsol scalar-relativistic norm-conserving pseudopotentials including non-linear core correction (NLCC) [39]. First, we have considered systems with a single conduction/valence band within an energy window of 0.25 eV above/below the minimum/maximum. The motivation is that spin-orbit coupling (SOC) has been shown to have a significant impact on phonon-limited mobilities [22]. Restricting our database to systems with a single band allows us to avoid the worst-case scenario of degenerate hole states that are split by SOC although it is clear that a proper treatment of relativistic effects in mobility calculations would require the inclusion of SOC effects both at the electronic and vibrational level. Secondly, we have considered only space groups for which the dynamical quadrupoles Q^* are zero by symmetry [40]. As recently shown in Refs. [4, 5, 22, 41, 42], dynamical quadrupoles play a crucial role for obtaining reliable phonon-limited mobilities in semiconductors. Unfortunately, the DFPT computation of Q^* is presently limited to norm-conserving pseudopotentials without NLCC, hence we decided to restrict the discussion to high-symmetry structures. Overall, our screening criteria led to 54 materials (37 in the Fm$\bar{3}$m space group, 16 in Pm$\bar{3}$m and one belonging to the tetragonal P4/mmm space group) and 67 mobilities (54 electron and 13 hole mobilities). Although our dataset mostly consists of cubic systems, we expect our analysis to hold for other structures as well.

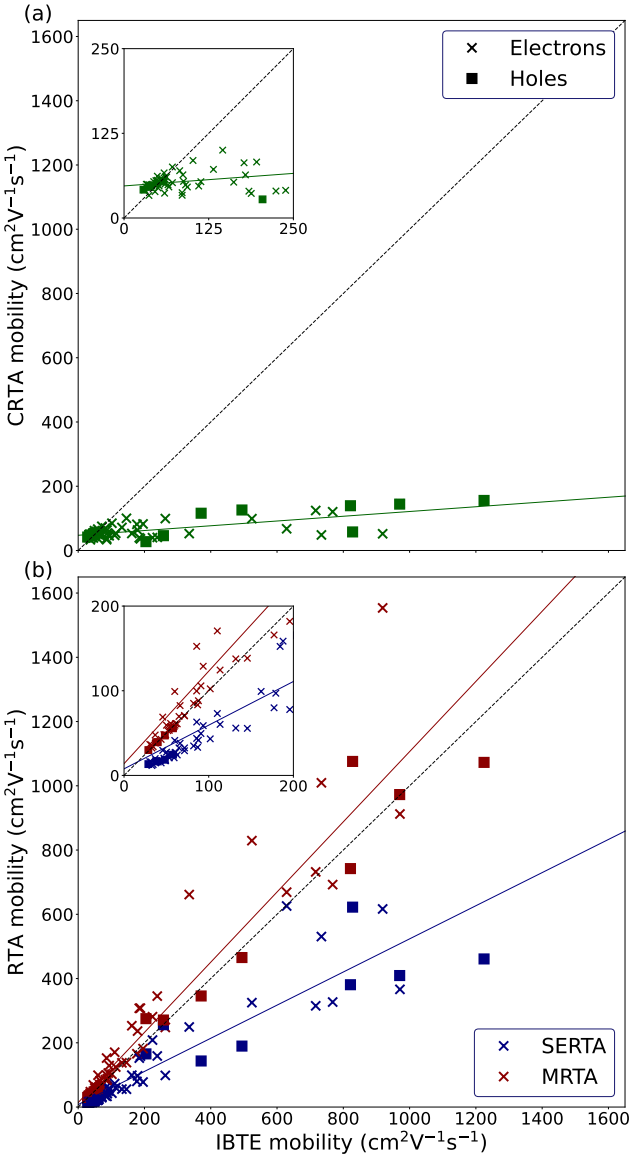

FIG. 1. Comparison of the (a) CRTA, and (b) SERTA, MRTA with the IBTE electron mobilities at 300 K. For the CRTA, the chosen lifetime minimizes the mean absolute error. MRTA mobilities are in red whereas SERTA mobilities are in blue. The black dotted lines represent the IBTE results. The green, blue, and red solid lines are linear fits of the CRTA, SERTA, and MRTA results, respectively.

Using our automated mobility computations, we can compare the SERTA, MRTA, and CRTA results versus the exact IBTE ones in a systematic way. Figure 1 shows this comparison of the CRTA (a) and SERTA/MRTA (b) mobilities with the IBTE results for all the systems in our dataset at 300 K. The numerical results can be found in Table S1 of the Supplemental Material [43]. Obviously, the CRTA mobility for a given material can be made exactly equal to the IBTE value by an appropriate choice of τ. In our dataset, a wide variety of lifetimes would

have to be used ranging from 7 fs for CsBr to 188 fs for $KMgH_3$. Considering the complete set of materials, a lifetime of 10.6 fs minimizes the mean absolute percentage error but, as can be seen from Fig. 1(a), the agreement with the IBTE is only valid for low IBTE mobilities, as most of the systems in the dataset have an IBTE mobility lower than 100 $cm^2V^{-1}s^{-1}$ (see the insets of Fig. 1). However, even in this region, a material with a low CRTA mobility may show a large relative error (see Fig. S1 of the Supplemental Material [43]). It is clear from Fig. 1(a) that the correlation is weak between the CRTA and IBTE results. A large (low) CRTA result does not guarantee a large (low) IBTE mobility. One can also compute Spearman's rank correlation coefficient ρ in order to quantify the ranking capability of CRTA. A value of $\rho^{\mathrm{CRTA}} = 0.45$ is obtained, indicating that the CRTA is overall not able to correctly rank materials from our dataset. This analysis therefore highlights the importance of going beyond the CRTA for accurate results. In particular, in material screening or high-throughput computing where this approach has been very popular, this indicates that the CRTA mobility or, equivalently, the transport effective mass [30, 33], should be used with extreme caution as a first filter to identify materials with high mobility and should be followed by a higher-level analysis of the transport if possible.

It is clear from Fig. 1(b) that the SERTA and MRTA both perform better than the CRTA. In particular, in terms of ranking materials of our dataset, both of them prove to be adequate, with $\rho^{\mathrm{SERTA}} = 0.97$ and $\rho^{\mathrm{MRTA}} = 0.98$. Additionally, Fig. 1(b) shows that the MRTA performs overall better than the SERTA in approximating the IBTE, with a mean absolute percentage error of 18% for the former and 48% for the latter. In the materials investigated here, the MRTA mobility is always higher than the one predicted by the SERTA. Indeed, we specifically selected materials with a single band, that is often located around Γ in the BZ. In this case, intravalley scattering largely dominates, in particular with small wave vectors $\mathbf{q}$ because the effective masses are lower than 1, hence the bands are relatively dispersive [4]. Note that intravalley scattering plays a crucial role even in cases where the band extrema are not at Γ. If the important wave vectors $\mathbf{q}$ are small, then α^{MRTA} is between 0 and 1, and the mobility increases from the SERTA to the MRTA. However, when compared to the IBTE, there is no general rule for the MRTA and it can underestimate or overestimate the mobility implying that the efficiency factor shown in Eq. (5) may under or overestimate the back-scattering events. Since our results were performed at 300 K, some deviations could be observed at higher/lower temperatures [16, 17]. However, we do not expect significant changes in the trends and these small differences seems dependent on the material investigated as shown in Fig. S2 and S3 of the Supplemental Material [43].

In the literature, SERTA has recently emerged as the most satisfactory approach. Indeed, for the few systems investigated so far (such as Si [4, 12, 25] or GaAs [4, 44]), it is predicted that the SERTA mobilities are closer to experimental data than the MRTA or IBTE results. Indeed, in Si, the differences between the SERTA, MRTA, and IBTE mobilities are lower than 5%, all of them being very close to experimental data [4, 12, 25]. However, in GaAs, there is a large spread in the reported computed mobilities, which can partly be explained by the different transport formalisms used for the computations, since the SERTA (MRTA) underestimates (overestimates) the IBTE solution by 52% (4%) [4, 16]. Our results demonstrate that large and difficult to predict errors can be present when using SERTA or MRTA.

From Fig. 1 and Table S1, it is clear that some outliers show very important deviations from the IBTE mobility. For instance, in SrO, KH, $KMgH_3$ and MgO, the MRTA leads to errors larger than 60% when compared to the exact IBTE solution.

While MRTA is performing better than SERTA, it seems impossible to estimate when the MRTA approach will fail. This indicates that both the SERTA and MRTA can be unreliable for some specific systems and the IBTE should always be preferred. In particular, before comparing computed mobilities to experimental data, we believe it is crucial to first make sure that any approximation used in the process is reliable, or at least to quantify the error on the final quantity. We point out that using spatial and time-reversal symmetries, and a similar filtering method as presented in Ref. [4], solving the IBTE can be seen as a post-processing of the SERTA that does not lead to a significant increase of computational time nor memory. It is also worth noting that the type of charge carrier does not seem to affect these results.

The computed IBTE mobilities overestimate the experimental data, which is expected since other sources of scattering (e.g., impurity scattering) are completely ignored. In addition, most of the experimental mobilities reported in the literature are measured using the Hall effect and it is therefore necessary to weight computational results by a material-dependent Hall factor that typically ranges between 0.7 and 2 [22]. The inclusion of the Hall mobility in ABINIT is left for future work.

The computation of the phonon-limited mobility is a rather complex task involving many steps. It typically requires an important human time and intervention. As a result, its automation has only realized for very specific cases [45]. To fully automate all the different parts of the computation, including the convergence studies for the BZ sampling, we have developed a workflow within the AbiPy python package [46]. The main steps are schematically represented in Fig. 2, with more details given in the Supplemental Material [43]. The ingredients needed in Eq. (2) are the KS wave functions on the dense mesh for the electronic part (in purple in Fig. 2) and the DFPT scattering potentials and the interatomic force constants on a coarse mesh (typical of DFPT) for the phonon part (in blue in Fig. 2). The latter can be easily computed with another AbiPy workflow, although in this study we

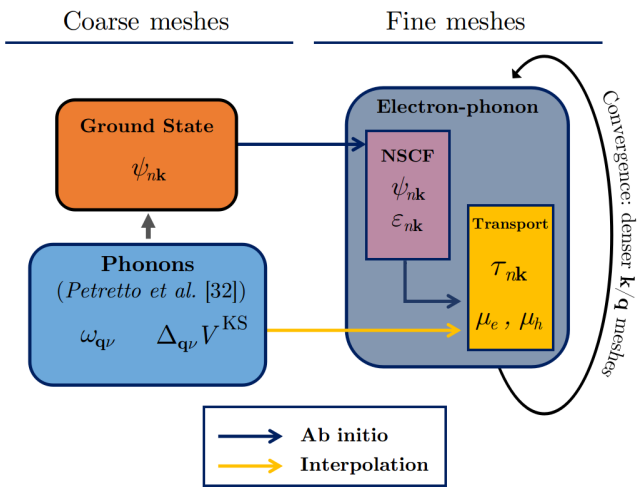

FIG. 2. Flowchart illustrating the workflow used to automatically compute phonon-limited mobilities.

prefer to start from a database of previous DFPT computations [37, 47]. The first step of the workflow consists in a ground-state calculation (in orange in Fig. 2), with basic parameters reused from the DFPT database. This allows to determine the wave functions on the fine mesh using a two-step procedure described in Ref. [4] and in the Supplemental Material [43]. All the ingredients required to compute the mobility on a given dense mesh are then readily available. Since a convergence study is needed with respect to this dense mesh, we perform the previous steps multiple times for meshes of increasing density. Convergence is assumed to be reached when three consecutive grids lead to mobilities maximum 5% away from each other.

In conclusion, we have obtained well-converged phonon-limited mobilities for a rather large set of semiconductors. We have developed and used an automatic workflow that allows for the comparison of different approximations to the BTE with the exact results. Our results show that SERTA and to a lesser degree MRTA are not reliable in general and that they are in many cases not good approximations to the IBTE. This should be kept in mind when looking at previously-published results using any of these approaches. The fact that the SERTA/MRTA agree with experiments for a few systems is not sufficient to establish these methods as a standard. Given that IBTE does not require more computational power, it should be the recommended approach for computing transport properties. Finally, our work demonstrates that phonon-limited mobilities can be computed automatically in a high-throughput manner, opening new avenues for materials screening.

ACKNOWLEDGMENT

G.-M. R. acknowledges financial support from F.R.S.-FNRS. Computational resources have been provided by the Consortium des Équipements de Calcul Intensif (CÉCI), funded by the Fonds de la Recherche Scientifique de Belgique (F.R.S.-FNRS) under Grant No. 2.5020.11 and by the Walloon Region. The present research benefited from computational resources made available on the Tier-1 supercomputer of the Fédération Wallonie-Bruxelles, infrastructure funded by the Walloon Region under grant agreement n°1117545. G.H. acknowledges funding by the U.S. Department of Energy, Office of Science, Office of Basic Energy Sciences, Materials Sciences and Engineering Division, under Contract DE-AC02-05-CH11231: Materials Project program KC23MP. The work has received partial support from the European Union's Horizon 2020 research and innovation program, grant agreement N° 951786 through the Center of Excellence NOMAD (NOMAD CoE).

[1] F. Giustino, M. L. Cohen, and S. G. Louie, Phys. Rev. B **76**, 165108 (2007).
[2] S. Poncé, E. R. Margine, C. Verdi, and F. Giustino, Comput. Phys. Commun. **209**, 116 (2016).
[3] J.-J. Zhou, J. Park, I.-T. Lu, I. Maliyov, X. Tong, and M. Bernardi, Comput. Phys. Commun. **264**, 107970 (2021).
[4] G. Brunin, H. P. C. Miranda, M. Giantomassi, M. Royo, M. Stengel, M. J. Verstraete, X. Gonze, G.-M. Rignanese, and G. Hautier, Phys. Rev. B **102**, 094308 (2020).
[5] G. Brunin, H. P. C. Miranda, M. Giantomassi, M. Royo, M. Stengel, M. J. Verstraete, X. Gonze, G.-M. Rignanese, and G. Hautier, Phys. Rev. Lett. **125**, 136601 (2020).
[6] X. Gonze, B. Amadon, G. Antonius, F. Arnardi, L. Baguet, J.-M. Beuken, J. Bieder, F. Bottin, J. Bouchet, E. Bousquet, *et al.*, Comput. Phys. Commun. **248**, 107042 (2020).
[7] A. H. Romero, D. C. Allan, B. Amadon, G. Antonius, T. Applencourt, L. Baguet, J. Bieder, F. Bottin, J. Bouchet, E. Bousquet, *et al.*, J. Chem. Phys. **152**, 124102 (2020).
[8] S. Poncé, W. Li, S. Reichardt, and F. Giustino, Rep. Prog. Phys. **83**, 036501 (2020).
[9] X. Gonze and C. Lee, Phys. Rev. B **55**, 10355 (1997).
[10] S. Baroni, S. de Gironcoli, A. Dal Corso, and P. Giannozzi, Rev. Mod. Phys. **73**, 515 (2001).
[11] A. M. Ganose, J. Park, A. Faghaninia, R. Woods-Robinson, K. A. Persson, and A. Jain, Nat. Commun. **12**, 1 (2021).
[12] S. Poncé, E. R. Margine, and F. Giustino, Phys. Rev. B **97**, 121201 (2018).
[13] I.-T. Lu, J.-J. Zhou, and M. Bernardi, Phys. Rev. Mat. **3**, 033804 (2019).
[14] I.-T. Lu, J. Park, J.-J. Zhou, and M. Bernardi, npj Comput. Mater. **6**, 1 (2020).
[15] I.-T. Lu, J.-J. Zhou, J. Park, and M. Bernardi, Phys. Rev. Mat. **6**, L010801 (2022).

[16] T.-H. Liu, J. Zhou, B. Liao, D. J. Singh, and G. Chen, Phys. Rev. B **95**, 075206 (2017).
[17] J. Ma, Y. Chen, and W. Li, Physical Review B **97**, 205207 (2018).
[18] T.-H. Liu, B. Song, L. Meroueh, Z. Ding, Q. Song, J. Zhou, M. Li, and G. Chen, Physical Review B **98**, 081203 (2018).
[19] J. M. Ziman, *Principles of the theory of solids*, 2nd ed. (Cambridge University Press, 1972).
[20] F. J. Blatt, in *Solid State Phys.*, Vol. 4 (Elsevier, 1957) pp. 199–366.
[21] F. Giustino, Rev. Mod. Phys. **89**, 015003 (2017).
[22] S. Poncé, F. Macheda, E. R. Margine, N. Marzari, N. Bonini, and F. Giustino, Phys. Rev. Research **3**, 043022 (2021).
[23] S. Li, Z. Tong, X. Zhang, and H. Bao, Physical Review B **102**, 174306 (2020).
[24] S. Li, A. Wang, Y. Hu, X. Gu, Z. Tong, and H. Bao, Materials Today Physics **15**, 100256 (2020).
[25] J. Ma, A. S. Nissimagoudar, and W. Li, Phys. Rev. B **97**, 045201 (2018).
[26] W. Li, Phys. Rev. B **92**, 075405 (2015).
[27] G. K. H. Madsen and D. J. Singh, Comput. Phys. Commun. **175**, 67 (2006).
[28] G. K. H. Madsen, J. Carrete, and M. J. Verstraete, Comput. Phys. Commun. **231**, 140 (2018).
[29] G. Hautier, A. Miglio, G. Ceder, G.-M. Rignanese, and X. Gonze, Nat. Commun. **4**, 1 (2013).
[30] F. Ricci, W. Chen, U. Aydemir, G. J. Snyder, G.-M. Rignanese, A. Jain, and G. Hautier, Sci. Data. **4**, 1 (2017).
[31] F. Ricci, A. Dunn, A. Jain, G.-M. Rignanese, and G. Hautier, J. Mater. Chem. A **8**, 17579 (2020).
[32] A. Faghaninia, G. Yu, U. Aydemir, M. Wood, W. Chen, G.-M. Rignanese, G. J. Snyder, G. Hautier, and A. Jain, Phys. Chem. Chem. Phys. **19**, 6743 (2017).
[33] G. Brunin, F. Ricci, V.-A. Ha, G.-M. Rignanese, and G. Hautier, npj Comput. Mater. **5**, 1 (2019).
[34] Z. M. Gibbs, F. Ricci, G. Li, H. Zhu, K. Persson, G. Ceder, G. Hautier, A. Jain, and G. J. Snyder, npj Comput. Mater. **3**, 1 (2017).
[35] D. M. Smiadak, R. Claes, N. Perez, M. Marshall, W. Peng, W. Chen, G. Hautier, G. Schierning, and A. Zevalkink, Mater. Today Phys. , 100597 (2022).
[36] R. Chmielowski, D. Péré, C. Bera, I. Opahle, W. Xie, S. Jacob, F. Capet, P. Roussel, A. Weidenkaff, G. K. Madsen, *et al.*, J. Appl. Phys. **117**, 125103 (2015).
[37] G. Petretto, S. Dwaraknath, H. P. C. Miranda, D. Winston, M. Giantomassi, M. J. Van Setten, X. Gonze, K. A. Persson, G. Hautier, and G. M. Rignanese, Sci. Data. **5**, 1 (2018).
[38] A. Jain, S. P. Ong, G. Hautier, W. Chen, W. D. Richards, S. Dacek, S. Cholia, D. Gunter, D. Skinner, G. Ceder, *et al.*, APL Mater. **1**, 011002 (2013).
[39] M. J. van Setten, M. Giantomassi, E. Bousquet, M. J. Verstraete, D. R. Hamann, X. Gonze, and G.-M. Rignanese, Comput. Phys. Commun. **226**, 39 (2018).
[40] Dynamical quadrupoles are non-zero in all non-centrosymmetric crystals, but also in centrosymmetric ones if one or more atoms are placed at non-centrosymmetric sites.
[41] V. A. Jhalani, J.-J. Zhou, J. Park, C. E. Dreyer, and M. Bernardi, Phys. Rev. Lett. **125**, 136602 (2020).
[42] J. Park, J.-J. Zhou, V. A. Jhalani, C. E. Dreyer, and M. Bernardi, Phys. Rev. B **102**, 125203 (2020).
[43] See Supplemental Material at `http://link` for more information about computational details and results,.
[44] J.-J. Zhou and M. Bernardi, Phys. Rev. B **94**, 201201 (2016).
[45] T. Sohier, D. Campi, N. Marzari, and M. Gibertini, Phys. Rev. Mat. **2**, 114010 (2018).
[46] M. Giantomassi *et al.*, "AbiPy project," `https://github.com/abinit/abipy`.
[47] G. Petretto, X. Gonze, G. Hautier, and G.-M. Rignanese, Comput. Mater. Sci. **144**, 331 (2018).
[48] D. G. Shankland, Int. J. Quantum Chem. **5**, 497 (1971).
[49] R. N. Euwema, D. J. Stukel, T. C. Collins, J. S. DeWitt, and D. G. Shankland, Phys. Rev. **178**, 1419 (1969).
[50] D. D. Koelling and J. H. Wood, J. Comput. Phys. **67**, 253 (1986).